Mathematical Models and Methods in Applied Sciences
Vol. 16, No. 8 (2006) 1347–1373

World Scientific
www.worldscientific.com

RECONSTRUCTION OF SINGULAR SURFACES BY SHAPE SENSITIVITY ANALYSIS AND LEVEL SET METHOD

GUILLAUME BAL* and KUI REN†

Department of Applied Physics and Applied Mathematics,
Columbia University, New York, NY 10027, USA
**gb2030@columbia.edu*
†*kr2002@columbia.edu*

Received 30 March 2005
Revised 11 October 2005
Communicated by N. Bellomo

We consider the reconstruction of singular surfaces from the over-determined boundary conditions of an elliptic problem. The problem arises in optical and impedance tomography, where void-like structure or cracks may be modeled as diffusion processes supported on co-dimension one surfaces. The reconstruction of such surfaces is obtained theoretically and numerically by combining a shape sensitivity analysis with a level set method. The shape sensitivity analysis is used to define a velocity field, which allows us to update the surface while decreasing a given cost function, which quantifies the error between the prediction of the forward model and the measured data. The velocity field depends on the geometry of the surface and the tangential diffusion process supported on it. The latter process is assumed to be known in this paper. The level set method is next applied to evolve the surface in the direction of the velocity field. Numerical simulations show how the surface may be reconstructed from noisy estimates of the full, or local, Neumann-to-Dirichlet map.

Keywords: Diffusion equations; interface conditions; tangential diffusion process; optical tomography; clear layers; level set method; shape sensitivity analysis; inverse problems.

AMS Subject Classification: 35J25, 35R30, 65N21

1. Introduction

The identification of unknown surfaces or interfaces in physical problems governed by partial differential equations has been an active field of research recently.[7,20,27] Apart from the fields of shape optimization and optimal design,[2,31] such problems emerge in applications such as optical tomography,[7,18] inverse scattering[28,35] and, more generally, parameter identification in partial differential equations.[12] Most works in the current literature deal with the reconstruction of interfaces that separate regions with different contrasts from boundary or far-field measurements, typically interfaces across which one of the constitutive parameters in the partial differential equation jumps.

In this paper, we study an inverse interface problem in which the role of the interface is not to separate regions with different physical coefficients but rather to be the support of a tangential diffusion process. Such a process may model thin areas characterized by very high values of the diffusion coefficient, as in the modeling of cracks of thickness $\varepsilon \ll 1$ and conductivity of order ε^{-1} in impedance tomography. It is known[25] that such cracks may be modeled by a tangential diffusion process supported on an interface. Another application is the modeling of clear layers in optical tomography. Optical tomography consists of probing human tissues with near-infrared photons.[4] Classical diffusion equations are known to be valid away from clear layers.[5,22,34] The results obtained before[6,8] show that clear layers may also be modeled as a tangential diffusion process supported on a co-dimension one surface. In both applications, we thus have a second-order diffusion equation with possibly spatially varying diffusion coefficient, which we assume to be known, along with a singular diffusion process supported on an interface, which we want to reconstruct from over-determined boundary measurements.

In the absence of general analytic formulas, the inverse interface problem is usually solved by minimizing an objective function that measures the mismatch between the model predictions and the measurements. A central element in the minimization procedure is the calculation of the gradient of the objective function with respect to the variations in the shape of the interface. This is the shape sensitivity analysis.[24,39] Another important element in the minimization procedure is a numerical tool that is used to advect the interface once a suitable descent direction has been obtained by shape sensitivity analysis. As in the pioneering work by Santosa[35] and subsequent works mentioned in the review paper by Burger and Osher,[11] the level set method[11,29] may be used to that purpose. This paper generalizes the combination of a shape sensitivity analysis and level set method to the reconstruction of surfaces supporting singular diffusion processes from boundary measurements.

The rest of the paper is structured as follows. After introducing the singular interface problem and the related inverse problem in Sec. 2, we perform the shape sensitivity analysis in Sec. 3. In Sec. 4 we show how to choose a direction of descent that allows us to move the interface in such a way that the mismatch between the model predictions and the measurements decreases. We present in Sec. 5 a numerical algorithm for the singular surface reconstruction based on the level set method. Numerical reconstructions using synthetic data in academic geometries are presented in Sec. 6. A comparison with the reconstruction of interfaces separating domains with different diffusion constants[35] is also provided. Section 7 concludes the paper.

2. The Singular Surface Problem

2.1. *Forward model*

Let $\Omega \subset \mathbb{R}^n$ $(n = 2, 3)$ be a domain with Lipschitz boundary $\Gamma(\equiv \partial\Omega)$ and $\Sigma \subset \Omega$ a closed, non-self-intersecting, interface of class C^2 embedded in Ω and separating it

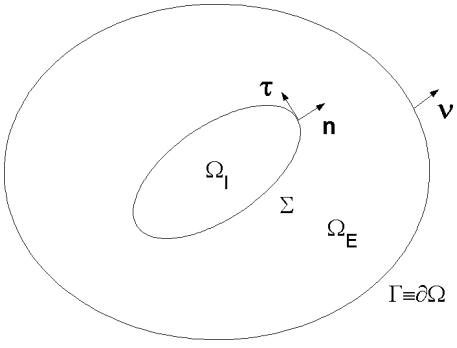

Fig. 1. Geometric setting of the problem in the two-dimensional setting with $\Omega = \Omega_I \cup \Omega_E \cup \Sigma$.

into interior (Ω_{I}) and exterior (Ω_{E}) parts, so that we may write $\Omega = \Omega_{\mathrm{I}} \cup \Omega_{\mathrm{E}} \cup \Sigma$. We also require that Σ stay away from $\partial\Omega$, i.e. $d(\Sigma, \Gamma) > C$ for some positive constant C. The geometry of interest is depicted in Fig. 1 in the two-dimensional setting. We consider the following elliptic partial differential equation in Ω with interface condition on Σ:

$$\begin{aligned} -\nabla \cdot \mathcal{D}(\mathbf{x})\nabla u(\mathbf{x}) + a(\mathbf{x})u(\mathbf{x}) &= 0 && \text{in } \Omega\backslash\Sigma, \\ \mathcal{D}(\mathbf{x})\nu(\mathbf{x}) \cdot \nabla u(\mathbf{x}) &= g(\mathbf{x}) && \text{on } \Gamma, \\ [u] &= 0 && \text{on } \Sigma, \\ [\mathbf{n} \cdot \mathcal{D}\nabla u] &= -\nabla_\perp \cdot d(\mathbf{x})\nabla_\perp u(\mathbf{x}) && \text{on } \Sigma. \end{aligned} \tag{2.1}$$

The scalar (to simplify) diffusion coefficients $\mathcal{D}(\mathbf{x})$ and $d(\mathbf{x})$ are uniformly positive; the absorption coefficient $a(\mathbf{x})$ is assumed to be smooth and bounded from above and below by positive constants, i.e. $0 < c_1 < a(\mathbf{x}) < c_2 < \infty$; $\mathbf{n}(\mathbf{x})$ is the outward unit normal vector to Ω_{I} at $\mathbf{x} \in \Sigma$ and $\nu(\mathbf{x})$ is the outward unit outer normal vector to Ω at $\mathbf{x} \in \Gamma$. The tangential differential operator $\nabla_\perp$ is the restriction of ∇ to Σ, so that for a sufficiently smooth function $\phi(\mathbf{x})$ defined on Ω, we have $\nabla_\perp \phi(\mathbf{x}) = \nabla\phi(\mathbf{x}) - (\mathbf{n}(\mathbf{x}) \cdot \nabla\phi(\mathbf{x}))\mathbf{n}(\mathbf{x})$ for $\mathbf{x} \in \Sigma$. The symbol $\nabla_\perp \cdot \nabla_\perp$ denotes the Laplace–Beltrami operator on Σ. The jump conditions across the interface Σ are defined by

$$[u] = u(\mathbf{x}^+) - u(\mathbf{x}^-), \quad [\mathbf{n} \cdot \mathcal{D}\nabla u] = \mathbf{n} \cdot \mathcal{D}\nabla u(\mathbf{x}^+) - \mathbf{n} \cdot \mathcal{D}\nabla u(\mathbf{x}^-), \tag{2.2}$$

with

$$u(\mathbf{x}^\pm) = \lim_{t \to 0_+} u\big(\mathbf{x} \pm t\mathbf{n}(\mathbf{x})\big), \quad \nabla u(\mathbf{x}^\pm) = \lim_{t \to 0_+} \nabla u\big(\mathbf{x} \pm t\mathbf{n}(\mathbf{x})\big). \tag{2.3}$$

Equation (2.1) models a background diffusion-absorption process in the domain Ω with a tangential diffusion process supported on the surface Σ.[8,25]

The problem described in (2.1) is well-posed in the following Hilbert space:

$$H^1_\Sigma(\Omega) := \left\{ u(\mathbf{x}) : u \in H^1(\Omega), \text{ such that } \int_\Sigma |\nabla_\perp u|^2 d\sigma < \infty \right\}, \tag{2.4}$$

where $H^1(\Omega)$ is the usual Sobolev space of L^2 functions in the domain Ω whose first-order partial derivatives also in $L^2(\Omega)$.[1,16] In other words, $H^1_\Sigma(\Omega)$ consists of

functions in $H^1(\Omega)$ with tangential gradient on Σ in $L^2(\Sigma)$. One can verify that $H^1_\Sigma(\Omega)$ is a Hilbert space equipped with the scalar product:

$$(u,v)_{H^1_\Sigma} = \int_\Omega (uv + \nabla u \cdot \nabla v) d\mathbf{x} + \int_\Sigma \nabla_\perp u \cdot \nabla_\perp v d\sigma(\mathbf{x}), \tag{2.5}$$

where $d\sigma(\mathbf{x})$ denote the Lebesgue measure on Σ, and a natural norm

$$\|u\|_{H^1_\Sigma} = \sqrt{(u,u)_{H^1_\Sigma}}. \tag{2.6}$$

Upon multiplying (2.1) by a test function $\phi(\mathbf{x}) \in H^1_\Sigma(\Omega)$ and integrating by parts, we obtain that

$$S(u,\phi) = f_g(\phi), \tag{2.7}$$

where the bilinear form $S(\cdot,\cdot)$ is defined by

$$\begin{aligned} S(u,\phi) := &\int_\Omega \mathcal{D}(\mathbf{x}) \nabla u(\mathbf{x}) \cdot \nabla \phi(\mathbf{x}) d\mathbf{x} + \int_\Omega a(\mathbf{x}) u(\mathbf{x}) \phi(\mathbf{x}) d\mathbf{x} \\ &+ \int_\Sigma d(\mathbf{x}) \nabla_\perp u(\mathbf{x}) \cdot \nabla_\perp \phi(\mathbf{x}) d\sigma(\mathbf{x}), \end{aligned} \tag{2.8}$$

and the linear form $f_g(\phi)$ by

$$f_g(\phi) := \int_\Gamma g(\mathbf{x}) \phi(\mathbf{x}) d\sigma(\mathbf{x}). \tag{2.9}$$

Note that S is symmetric, i.e. $S(u,\phi) = S(\phi,u)$. Because the diffusion coefficients $\mathcal{D}(\mathbf{x})$ and $d(\mathbf{x})$ and the absorption coefficient $a(\mathbf{x})$ are positive and bounded, one can verify that the bilinear form S is coercive. It then follows from Lax–Milgram theory[16,23] that if $g \in H^{-1/2}(\Gamma)$, then (2.1) admits a unique solution $u \in H^1_\Sigma$ with trace on Γ, $u|_\Gamma \in H^{1/2}(\Gamma)$; see also Ref. 7.

2.2. *Inverse surface problem*

A practically useful inverse problem related to Eq. (2.1) consists of reconstructing the interface Σ from knowledge of u at the boundary Γ. The Neumann-to-Dirichlet (NtD) operator, which maps the incoming flux g to u on the boundary[26] is defined as:

$$\Lambda_\Sigma : \begin{array}{c} H^{-1/2}(\Gamma) \mapsto H^{1/2}(\Gamma) \\ g(\Gamma) \mapsto u|_\Gamma. \end{array} \tag{2.10}$$

This operator obviously depends on the geometry of Σ. The inverse interface problem of (2.1) may then be formulated as:

> (IP) Determine the interface Σ from knowledge of the Neumann-to-Dirichlet operator Λ_Σ.

If all the other coefficients in (2.1) are known, it is shown in a previous work[7] that knowledge of the local Neumann-to-Dirichlet map uniquely determines the interface Σ. Let us denote by $\Gamma_g \subset \Gamma$ the part of the boundary where nonzero boundary current are applied and measurements are taken. In other words, we replace the boundary condition of (2.1) by

$$\mathcal{D}(\mathbf{x})\nu(\mathbf{x}) \cdot \nabla u(\mathbf{x}) = \begin{cases} g(\mathbf{x}), & \text{on } \Gamma_g \\ 0, & \text{on } \Gamma \backslash \Gamma_g. \end{cases} \tag{2.11}$$

Denoting by $\Lambda_\Sigma^{\Gamma_g}$ the local Neumann-to-Dirichlet operator for the new problem, which implies that u is measured only on Γ_g. Then we have the following uniqueness result[7]:

Proposition 2.1. *Let $\Lambda_{\Sigma_1}^{\Gamma_g}$ and $\Lambda_{\Sigma_2}^{\Gamma_g}$ be the local NtD maps associated with interfaces Σ_1 and Σ_2, respectively. Suppose that the functions $\mathcal{D}(\mathbf{x})$, $d(\mathbf{x})$ and $a(\mathbf{x})$ are known and satisfy the above mentioned regularity assumptions. Then $\Lambda_{\Sigma_1}^{\Gamma_g} = \Lambda_{\Sigma_2}^{\Gamma_g}$ implies that $\Sigma_1 = \Sigma_2$.*

The objective of this paper is to design a numerical method to reconstruct the singular interface Σ from knowledge of Λ_Σ or $\Lambda_\Sigma^{\Gamma_g}$. Our method is based on classical numerical optimization techniques. We convert the reconstruction problem to a regularized nonlinear least square problem:

$$\mathcal{F}_\alpha(\Sigma) := \frac{1}{2}\left\|u - u_m^\delta\right\|_{L^2(\Gamma)}^2 + \alpha \int_\Sigma d\sigma(\mathbf{x}) \to \min_{\Sigma \in \Pi}. \tag{2.12}$$

Here u_m^δ denotes a noisy measurement of u on the domain boundary Γ with noise level δ, while Π denotes the space of admissible surfaces Σ. The first term in the objective functional $\mathcal{F}_\alpha(\Sigma)$ evaluates the discrepancy between the measured and predicted data, while the second term is a regularization term with parameter α. The choice of set Π is critical to the existence of minimizers to the functional $\mathcal{F}_\alpha(\Sigma)$. If we assume that Π consists of interfaces such that $\int_\Sigma d\sigma(\mathbf{x})$ is the $(n-1)$-dimensional Hausdorff measure of Σ, which turns out to be the perimeter of the inner domain Ω_I in two dimensions, we can then view the reconstruction of Σ as the identification of the domain Ω_I penalized by its perimeter. By techniques such as those of Ambrosio and Buttazzo,[3] Dal Maso and Toader,[15] the existence of minimizer to functional $\mathcal{F}_\alpha$ should follow from the lower semicontinuity of $\mathcal{F}_\alpha(\Sigma)$ with respect to Ω_I (thus Σ) in either the space of sets with finite parameter or the space of simply-connected, Hausdorff measurable compact sets. For our analysis below, we need interfaces that are at least of class C^2 such that the mean curvature of the interfaces can be defined in the classical way. It is, however, not clear to us so far that a minimizer of $\mathcal{F}_\alpha$ exists in such a class of interfaces. Our analysis in the following sections are thus based on the assumption that a regular minimizer does exists.

In many applications, such as the reconstruction of clear layers in optical tomography, we may have *a priori* information about the location of the singular

interface, whence constraints on the size of Π, which may simplify the inverse problem. We do not consider this situation here.

2.3. *Comparison with the reconstruction of inclusions*

It is instructive to compare the reconstruction of singular surfaces as they are described in the preceding section with the more classical problem of the reconstruction of interfaces separating regions characterized by different diffusion coefficients.[27,28,35] In the latter works, the inclusion is characterized by a constant diffusion coefficient that differs from the constant background diffusion coefficient. The inclusion is then reconstructed by minimizing the functional (2.12). The construction of velocity fields allowing us to minimize (2.12) is not modified when the inclusion's and background diffusion coefficients are allowed to be (not necessarily constant) smooth functions, so long as the difference between these functions does not vanish. More precisely, we consider the following model for the inclusions:

$$\begin{aligned} -\nabla\cdot\mathcal{D}(\mathbf{x})\nabla u(\mathbf{x}) + a(\mathbf{x})u(\mathbf{x}) &= 0 \qquad \text{in } \Omega,\\ \mathcal{D}(\mathbf{x})\nu(\mathbf{x})\cdot\nabla u(\mathbf{x}) &= g(\mathbf{x}) \qquad \text{on } \Gamma,\\ [u] &= 0 \qquad \text{on } \Sigma,\\ [\mathbf{n}\cdot\mathcal{D}\nabla u] &= 0 \qquad \text{on } \Sigma, \end{aligned} \tag{2.13}$$

where the diffusion coefficient $\mathcal{D}(\mathbf{x})$ jumps across the interface Σ

$$\mathcal{D}(\mathbf{x}) = \begin{cases} \mathcal{D}_0(\mathbf{x}) + \delta\mathcal{D}(\mathbf{x}) \equiv \mathcal{D}_I(\mathbf{x}), & \mathbf{x}\in\Omega_I,\\ \mathcal{D}_0(\mathbf{x}) \equiv \mathcal{D}_E(\mathbf{x}), & \mathbf{x}\in\Omega_E, \end{cases} \tag{2.14}$$

with $\mathcal{D}(\mathbf{x})$ uniformly bounded from above and below by positive constants and $\delta\mathcal{D}(\mathbf{x})$ strictly positive or strictly negative. The case where $\mathcal{D}_0$ and $\delta\mathcal{D}$ are constant has been studied extensively.[27,28,35] The behavior of the solution $u(\mathbf{x})$ to (2.1) with $d(\mathbf{x}) > 0$ is very similar to the behavior of solution of model (2.13) with $\delta D(\mathbf{x}) > 0$. In Sec. 6, we will give a more quantitative numerical comparison between the two models.

3. Shape Sensitivity Analysis

In order to solve the surface reconstruction problem by minimization of the functional $\mathcal{F}_\alpha(\Sigma)$ in (2.12), it is essential to compute the variation of $\mathcal{F}_\alpha(\Sigma)$ with respect to a small perturbation in Σ. This involves computing the sensitivity of the diffusion solution with respect to deformations in the shape. This is the shape sensitivity analysis described in the shape optimization literature.[39]

The main novelty of the paper is to carry out the shape sensitivity analysis in the presence of a singular interface. Unlike the model (2.13) treated before,[27,28,35] the current jumps across the interface Σ in (2.1). This significantly modifies the shape sensitivity analysis and the important relationship between shape and material derivatives; see below. Let us also mention that many geometries have been

addressed in the shape optimization literature.[17,21,38,39] Because of the specificity of problem (2.1), none of them may be applied directly, although similarities in the methodology and mathematical machinery are easily drawn.

The framework for the shape sensitivity analysis is the following. We perturb the interface Σ according to the map $\mathbf{F}_t : \mathbb{R}^n \to \mathbb{R}^n$ (the parameter $t \in \mathbb{R}^+$ is a small positive real number) defined by:

$$\mathbf{F}_t(\mathbf{x}) = \mathbf{x} + t\mathbf{V}(\mathbf{x}), \quad \mathbf{x} \in \mathbb{R}^n. \tag{3.1}$$

Here $\mathbf{V}(\mathbf{x}) : \mathbb{R}^n \mapsto \mathbb{R}^n$ is a vector field of class C^1 with compact support in the domain Ω so that each point on the boundary of Ω remains invariant under the perturbation $\mathbf{F}_t$. We denote this as $\mathbf{V} \in C_0^1(\Omega; \mathbb{R}^n)$. Under this perturbation, points $\mathbf{x} \in \Omega$ are mapped to $\mathbf{x} + t\mathbf{V}(\mathbf{x})$. However, the whole domain Ω remains invariant in the sense that $\Omega = \mathbf{F}_t(\Omega)$.

We denote by Σ_t the image of Σ under the perturbation, and denote by $u_t(\mathbf{x})$ the solution of problem (2.1) with Σ replaced by the perturbed interface Σ_t. The variation of u with respect to variations in the interface Σ is called the *shape derivative* of u with respect to Σ. More precisely:

Definition 3.1. (Shape derivative) Let $u \in H^1_\Sigma$ and $u_t \in H^1_{\Sigma_t}$ be solutions of problem (2.1) with interface Σ and Σ_t, respectively. Assume that $\mathbf{V} \in C_0^1(\Omega; \mathbb{R}^n)$ be a vector field given in (3.1). If the limit

$$u'(\Sigma; \mathbf{V}) := \lim_{t \to 0} \frac{u_t - u}{t} \tag{3.2}$$

exists in the strong (weak) topology of some Banach space of functions $B(\Omega)$, then we call $u'(\Sigma; \mathbf{V})$ the strong (weak) shape derivative of u in direction $\mathbf{V}$.

We refer to Remark 3.3 below for a remark on the choice of a Banach space and a topology. The calculation of $u'(\Sigma; \mathbf{V})$ is greatly simplified by the introduction of a *material derivative*[39]:

Definition 3.2. (Material derivative) Let $u \in H^1_\Sigma$, $u_t \in H^1_{\Sigma_t}$ and $\mathbf{V}$ be given as in Definition 3.1, and define $u^t = u_t \circ \mathbf{F}_t$. If the limit

$$\dot{u}(\Sigma; \mathbf{V}) := \lim_{t \to 0} \frac{u^t - u}{t} \tag{3.3}$$

exists in the strong (weak) topology of some Banach space of functions $B(\Omega)$, we call $\dot{u}(\Sigma; \mathbf{V})$ the strong (weak) material derivative of u in direction $\mathbf{V}$.

We also refer to Remark 3.3 for the choice of a Banach space and a topology. The material derivative thus quantifies the variations of u with respect to changes in the geometry for a moving (Lagrangian) coordinate system. The shape and material

derivatives introduced in Definitions 3.1 and 3.2, respectively, are not independent of each other. More precisely, we have[39]:

$$u'(\Sigma;\mathbf{V}) = \dot{u}(\Sigma;\mathbf{V}) - \mathbf{V}\cdot\nabla u, \tag{3.4}$$

provided that both $\dot{u}(\Sigma;\mathbf{V})$ and $\mathbf{V}\cdot\nabla u$ make sense. This relation tells us that in order to compute the shape derivative of u, we can compute the material derivative first and then use (3.4) to obtain the shape derivative.

3.1. *The material derivatives*

Before we compute the material derivatives of u for model (2.1), we need to introduce some notation. We will denote by $(\cdot,\cdot)_{(X)}$ the inner product of space $L^2(X)$:

$$(x,y)_{(X)} := \int_X x\cdot y d\mu, \tag{3.5}$$

with $d\mu$ the Lebesgue measure on a domain X. For any vector quantity $\mathbf{Y}$ on the interface, we use $Y_n\mathbf{n} \equiv (\mathbf{n}\cdot\mathbf{Y})\mathbf{n}$ and $\mathbf{Y}_\perp \equiv \mathbf{Y} - (\mathbf{n}\cdot\mathbf{Y})\mathbf{n}$ to denote the normal and tangential components of $\mathbf{Y}$, respectively.

We now examine the variations of the solution to the diffusion equation (2.1) when the interface Σ_t varies. We first observe that u_t satisfies the following relation:

$$(\mathcal{D}\nabla u_t, \nabla\phi_t)_{(\Omega)} + (au_t,\phi_t)_{(\Omega)} + (d\nabla_\perp u_t, \nabla_\perp\phi_t)_{(\Sigma_t)} = f_g(\phi_t), \tag{3.6}$$

for all $\phi_t \in H^1_{\Sigma_t}(\Omega)$. We introduce

$$J_t = \det(\mathbf{DF}_t) \quad \text{and} \quad \mathbf{A}_t = \mathbf{DF}_t^{-1}\mathbf{DF}_t^{-*}, \tag{3.7}$$

with the superscript * denoting the transpose operation and superscript $^{-*}$ denoting the transpose of the inverse. The Jacobi matrix of the transformation $\mathbf{F}_t$ is denoted by $\mathbf{DF}_t$. The strong continuity of the (matrix) functions J_t, $\mathbf{A}_t$, and $\mathbf{F}_t$ and the following identities can be verified[39]

$$(\nabla u_t)\circ\mathbf{F}_t = (\mathbf{DF}_t^{-*})\nabla u^t, \quad J_t|_{t=0} = 1, \quad \mathbf{A}_t|_{t=0} = \mathbf{I}, \tag{3.8}$$

$$\frac{d}{dt}\mathbf{F}_t|_{t=0} = \mathbf{V}, \quad \frac{d}{dt}(\mathbf{DF}_t)|_{t=0} = \mathbf{DV}, \quad \frac{d}{dt}(\mathbf{DF}_t^{-1})|_{t=0} = -\mathbf{DV}, \tag{3.9}$$

$$J_0' \equiv \frac{dJ_t}{dt}|_{t=0} = \nabla\cdot\mathbf{V},\ \mathbf{A}_0' \equiv \frac{d\mathbf{A}_t}{dt}|_{t=0} = -(\mathbf{DV} + (\mathbf{DV})^*). \tag{3.10}$$

Here $\mathbf{I}$ is the identity matrix.

We now replace $\nabla_\perp u_t$ on the interface Σ by $\nabla u_t^+ - (\mathbf{n}_t\cdot\nabla u_t^+)\mathbf{n}_t$. We could also replace it by $\nabla u_t^- - (\mathbf{n}_t\cdot\nabla u_t^-)\mathbf{n}_t$ and will show that the final result does not depend on the chosen expression, as it should; see for example (3.29) below. We thus recast (3.6) as

$$\begin{aligned}(\mathcal{D}\nabla u_t, \nabla\phi_t)_{(\Omega)} + (au_t,\phi_t)_{(\Omega)} + (d\nabla u_t^+, \nabla\phi_t^+)_{(\Sigma_t)}\\ - (d\mathbf{n}_t\cdot\nabla u_t^+, \mathbf{n}_t\cdot\nabla\phi_t^+)_{(\Sigma_t)} = f_g(\phi_t).\end{aligned} \tag{3.11}$$

Performing the change of variables $\mathbf{x} \mapsto \mathbf{F}_t(\mathbf{x})$ in the above equality yields

$$S_t(u^t, \phi^t) = f_g(\phi^t), \tag{3.12}$$

where $\phi^t = \phi_t \circ \mathbf{F}_t$ and $S_t(u^t, \phi^t)$ are given by

$$\begin{aligned} S_t(u^t, \phi^t) \equiv\ & (\mathcal{D}_{\mathbf{F}_t} J_t \mathbf{A}_t \nabla u^t, \nabla \phi^t)_{(\Omega)} + (a_{\mathbf{F}_t} J_t u^t, \phi^t)_{(\Omega)} \\ & + (d_{\mathbf{F}_t} \omega_t \mathbf{A}_t \nabla u^{+t}, \nabla \phi^{+t})_{(\Sigma)} - (d_{\mathbf{F}_t} \pi_t \mathbf{A}_t \mathbf{n} \cdot \nabla u^{+t}, \mathbf{A}_t \mathbf{n} \cdot \nabla \phi^{+t})_{(\Sigma)}, \end{aligned} \tag{3.13}$$

with $\mathcal{D}_{\mathbf{F}_t} \equiv \mathcal{D} \circ \mathbf{F}_t$, $a_{\mathbf{F}_t} \equiv a \circ \mathbf{F}_t$ and $d_{\mathbf{F}_t} \equiv d \circ \mathbf{F}_t$. The functions ω_t and π_t are defined as

$$\omega_t = J_t \|\mathbf{D}\mathbf{F}_t^{-*} \cdot \mathbf{n}\|_{\mathbb{R}^n}, \quad \pi_t = \frac{J_t}{\|\mathbf{D}\mathbf{F}_t^{-*} \cdot \mathbf{n}\|_{\mathbb{R}^n}} \tag{3.14}$$

with $\|\cdot\|_{\mathbb{R}^n}$ denoting the Euclidean norm in $\mathbb{R}^n$, and verify

$$\omega_0 = 1, \quad \pi_0 = 1, \tag{3.15}$$

$$\omega_0' \equiv \frac{d\omega_t}{dt}|_{t=0} = \nabla \cdot \mathbf{V} - \mathbf{n}^* \mathbf{D}\mathbf{V}\mathbf{n} \equiv \mathrm{div}_\Sigma \mathbf{V}, \tag{3.16}$$

$$\pi_0' \equiv \frac{d\pi_t}{dt}|_{t=0} = \nabla \cdot \mathbf{V} + \mathbf{n}^* \mathbf{D}\mathbf{V}\mathbf{n}. \tag{3.17}$$

Choosing the test function ϕ^t in (2.7), we then deduce from (3.12) and (2.7) that

$$S(u, \phi^t) = S_t(u^t, \phi^t). \tag{3.18}$$

On the other hand, we have for all ϕ, $\psi \in H^1_\Sigma(\Omega)$, the following result

$$\begin{aligned} S_t(\psi, \phi) - S(\psi, \phi) =\ & ((\mathcal{D}_{\mathbf{F}_t} - \mathcal{D}) J_t \mathbf{A}_t \nabla \psi, \nabla \phi)_{(\Omega)} + (\mathcal{D}(J_t \mathbf{A}_t - \mathbf{I}) \nabla \psi, \nabla \phi)_{(\Omega)} \\ & + ((a_{\mathbf{F}_t} - a) J_t \psi, \phi)_{(\Omega)} + (a(J_t - 1)\psi, \phi)_{(\Omega)} + ((d_{\mathbf{F}_t} - d)\omega_t \mathbf{A}_t \nabla \psi^+, \nabla \phi^+)_{(\Sigma)} \\ & + (d(\omega_t \mathbf{A}_t - \mathbf{I}) \nabla \psi^+, \nabla \phi^+)_{(\Sigma)} - ((d_{\mathbf{F}_t} - d)\pi_t \mathbf{A}_t \mathbf{n} \cdot \nabla \psi^+, \mathbf{A}_t \mathbf{n} \cdot \nabla \phi^+)_{(\Sigma)} \\ & - (d(\pi_t \mathbf{A}_t - \mathbf{I})\mathbf{n} \cdot \nabla \psi^+, \mathbf{A}_t \mathbf{n} \cdot \nabla \phi)_{(\Sigma)} - (d\mathbf{n} \cdot \nabla \psi^+, (\mathbf{A}_t - \mathbf{I})\mathbf{n} \cdot \nabla \phi^+)_{(\Sigma)}, \end{aligned} \tag{3.19}$$

which implies that

$$\begin{aligned} |S_t(\psi, \phi) - S(\psi, \phi)| \le\ & \frac{C_1(t)}{2}(\|\nabla \psi\|^2_{L^2(\Omega)} + \|\nabla \phi\|^2_{L^2(\Omega)}) \\ & + \frac{C_2(t)}{2}(\|\psi\|^2_{L^2(\Omega)} + \|\phi\|^2_{L^2(\Omega)}) \\ & + \frac{C_3(t)}{2}(\|\nabla \psi^+\|^2_{L^2(\Sigma)} + \|\nabla \phi^+\|^2_{L^2(\Sigma)}) \\ & + \frac{C_4(t)}{2}(\|\mathbf{n} \cdot \nabla \psi^+\|^2_{L^2(\Sigma)} + \|\mathbf{n} \cdot \nabla \phi^+\|^2_{L^2(\Sigma)}), \end{aligned} \tag{3.20}$$

with $C_1(t)$, $C_2(t)$, $C_3(t)$ and $C_4(t)$ given by

$$\begin{aligned}
C_1(t) &= \|(\mathcal{D}_{\mathbf{F}_t} - \mathcal{D})J_t\mathbf{A}_t\|_{L^\infty(\Omega)} + \|\mathcal{D}(J_t\mathbf{A}_t - \mathbf{I})\|_{L^\infty(\Omega)},\\
C_2(t) &= \|(a_{\mathbf{F}_t} - a)J_t\|_{L^\infty(\Omega)} + \|a(J_t - 1)\|_{L^\infty(\Omega)},\\
C_3(t) &= \|(d_{\mathbf{F}_t} - d)\omega_t\mathbf{A}_t\|_{L^\infty(\Omega)} + \|d(\omega_t\mathbf{A}_t - \mathbf{I})\|_{L^\infty(\Omega)},\\
C_4(t) &= \|(d_{\mathbf{F}_t} - d)\pi_t\mathbf{A}_t\|_{L^\infty(\Omega)}\|\mathbf{A}_t\|_{L^\infty(\Omega)}\\
&\quad + \|d(\pi_t\mathbf{A}_t - \mathbf{I})\|_{L^\infty(\Omega)}\|\mathbf{A}_t\|_{L^\infty(\Omega)} + \|\mathbf{A}_t - \mathbf{I}\|_{L^\infty(\Omega)}.
\end{aligned} \tag{3.21}$$

Here the norms $\|\cdot\|_{L^2}$ and $\|\cdot\|_{L^\infty}$ are the usual ones defined on vector (matrix) functions. Because of the strong continuity of $\mathbf{A}_t$, J_t, ω_t and π_t (as functions of t), we deduce the following result on S_t:

Lemma 3.1. *The bilinear form S_t is continuous with respect to the perturbation parameter t in* (3.1) *at $t = 0$, which means*

$$\lim_{t\to 0+} S_t(\cdot,\cdot) = S(\cdot,\cdot). \tag{3.22}$$

Let us recast the identity (3.18) as the following relation

$$T_1 + T_2 + T_3 - T_4 - T_5 = 0, \tag{3.23}$$

where the terms T_k are given by

$$\begin{aligned}
T_1 &= \left(\frac{\mathcal{D}_{\mathbf{F}_t} - \mathcal{D}}{t}J_t\mathbf{A}_t\nabla u^t + \mathcal{D}J_t\mathbf{A}_t\frac{\nabla u^t - \nabla u}{t} + \mathcal{D}\frac{J_t\mathbf{A}_t - \mathbf{I}}{t}\nabla u, \nabla\phi^t\right)_{(\Omega)},\\
T_2 &= \left(\frac{a_{\mathbf{F}_t} - a}{t}J_t u^t + aJ_t\frac{u^t - u}{t} + a\frac{J_t - 1}{t}u, \phi^t\right)_{(\Omega)},\\
T_3 &= \left(\frac{d_{\mathbf{F}_t} - d}{t}\omega_t\mathbf{A}_t\nabla u^{+t} + d\frac{\omega_t\mathbf{A}_t - \mathbf{I}}{t}\nabla u^{+t} + d\frac{\nabla u^{+t} - \nabla u^+}{t}, \nabla\phi^{+t}\right)_{(\Sigma)},\\
T_4 &= \left(\frac{d_{\mathbf{F}_t} - d}{t}\pi_t\mathbf{A}_t\mathbf{n}\cdot\nabla u^{+t} + d\frac{\pi_t\mathbf{A}_t - \mathbf{I}}{t}\mathbf{n}\cdot\nabla u^{+t}, \mathbf{A}_t\mathbf{n}\cdot\nabla\phi^{+t}\right)_{(\Sigma)},\\
T_5 &= \left(d\frac{\mathbf{n}\cdot\nabla u^{+t} - \mathbf{n}\cdot\nabla u^+}{t}, \mathbf{A}_t\mathbf{n}\cdot\nabla\phi^{+t}\right)_{(\Sigma)} + \left(d\mathbf{n}\cdot\nabla u^+, \frac{\mathbf{A}_t - \mathbf{I}}{t}\mathbf{n}\cdot\nabla\phi^{+t}\right)_{(\Sigma)}.
\end{aligned} \tag{3.24}$$

Thanks to the continuity of S_t at $t = 0$, we can take a limit $t \to 0$ in (3.23) and obtain the following equation for the material derivative of u:

$$\begin{aligned}
&(\mathbf{V}\cdot\nabla\mathcal{D}\nabla u, \nabla\phi)_{(\Omega)} + (\mathcal{D}\nabla\dot{u}, \nabla\phi)_{(\Omega)} + (\mathcal{D}(J_0'\mathbf{I} + \mathbf{A}_0')\nabla u, \nabla\phi)_{(\Omega)}\\
&\quad + (\mathbf{V}\cdot\nabla a u, \phi)_{(\Omega)} + (a\dot{u}, \phi)_{(\Omega)} + (aJ_0'u, \phi)_{(\Omega)}\\
&\quad + (\mathbf{V}_\perp\cdot\nabla_\perp d\nabla u^+, \nabla\phi^+)_{(\Sigma)} + (d(\omega_0'\mathbf{I} + \mathbf{A}_0')\nabla u^+, \nabla\phi^+)_{(\Sigma)}\\
&\quad + (d\nabla\dot{u}^+, \nabla\phi^+)_{(\Sigma)} - (\mathbf{V}_\perp\cdot\nabla_\perp d\mathbf{n}\cdot\nabla u^+, \mathbf{n}\cdot\nabla\phi^+)_{(\Sigma)}\\
&\quad - (d(\pi_0'\mathbf{I} + \mathbf{A}_0')\mathbf{n}\cdot\nabla u^+, \mathbf{n}\cdot\nabla\phi^+)_{(\Sigma)} - (d\mathbf{n}\cdot\nabla\dot{u}^+, \mathbf{n}\cdot\nabla\phi^+)_{(\Sigma)}\\
&\quad - (d\mathbf{n}\cdot\nabla u^+, \mathbf{A}_0'\mathbf{n}\cdot\nabla\phi^+)_{(\Sigma)} = 0.
\end{aligned} \tag{3.25}$$

Using the expressions for $\mathbf{A}_0'$, J_0', ω_0' and π_0', we can show that the following simplifications are possible:

$$(d(\omega_0'\mathbf{I}+\mathbf{A}_0')\nabla u^+,\nabla\phi^+)_{(\Sigma)}-(d(\pi_0'\mathbf{I}+\mathbf{A}_0')\mathbf{n}\cdot\nabla u^+,\mathbf{n}\cdot\nabla\phi^+)_{(\Sigma)}$$
$$-(d\mathbf{n}\cdot\nabla u^+,\mathbf{A}_0'\mathbf{n}\cdot\nabla\phi^+)_{(\Sigma)}\ (d\mathrm{div}_\Sigma\mathbf{V}\nabla_\perp u,\nabla_\perp\phi)_{(\Sigma)}+(d\mathbf{A}_0'\nabla_\perp u,\nabla_\perp\phi)_{(\Sigma)}, \tag{3.26}$$

where we have replaced $\nabla u^+-(\mathbf{n}\cdot\nabla u^+)\mathbf{n}$ by $\nabla_\perp u$. The quantity $\mathrm{div}_\Sigma\mathbf{V}$ is defined in (3.16). It can also be shown that

$$(\mathbf{V}_\perp\cdot\nabla_\perp d\nabla u^+,\nabla\phi^+)_{(\Sigma)}-(\mathbf{V}_\perp\cdot\nabla_\perp d\mathbf{n}\cdot\nabla u^+,\mathbf{n}\cdot\nabla\phi^+)_{(\Sigma)}$$
$$=(\mathbf{V}_\perp\cdot\nabla_\perp d\nabla_\perp u,\nabla_\perp\phi)_{(\Sigma)} \tag{3.27}$$

and

$$(d\nabla\dot{u}^+,\nabla\phi^+)_{(\Sigma)}-(d\mathbf{n}\cdot\nabla\dot{u}^+,\mathbf{n}\cdot\nabla\phi^+)_{(\Sigma)}=(d\nabla_\perp\dot{u},\nabla_\perp\phi)_{(\Sigma)}. \tag{3.28}$$

We can thus simplify (3.25) as

$$S(\dot{u},\phi)=-(\mathbf{V}\cdot\nabla\mathcal{D}\nabla u,\nabla\phi)_{(\Omega)}-(\mathcal{D}(J_0'\mathbf{I}+\mathbf{A}_0')\nabla u,\nabla\phi)_{(\Omega)}-(\nabla\cdot(a\mathbf{V})u,\phi)_{(\Omega)}$$
$$-(\mathbf{V}_\perp\cdot\nabla_\perp d\nabla_\perp u,\nabla_\perp\phi)_{(\Sigma)}-(d\mathrm{div}_\Sigma\mathbf{V}\nabla_\perp u,\nabla_\perp\phi)_{(\Sigma)}$$
$$-(d\mathbf{A}_0'\nabla_\perp u,\nabla_\perp\phi)_{(\Sigma)}. \tag{3.29}$$

We summarize the above results in the following theorem:

Theorem 3.1. *Let $\mathcal{D}(\mathbf{x})$, $a(\mathbf{x})$ and $d(\mathbf{x})$ be functions of class C^1. Then the material derivative $\dot{u}\in H^1_\Sigma(\Omega)$ of the solution $u\in H^1_\Sigma(\Omega)$ to* (2.1) *in direction $\mathbf{V}$ is the unique solution to* (3.29)*. Moreover, we verify that*

$$[\dot{u}]=0\quad \textit{on } \Sigma. \tag{3.30}$$

The condition (3.30) comes from the third identity in (2.1).

3.2. *The shape derivative*

The shape derivative of u can be computed by using (3.4). However, before we proceed to computing it, we stress that u' can no longer be an element of H^1_Σ. The jump of the normal derivative of u across the interface Σ causes a discontinuity of the tangential derivative of u' across the interface according to formula (3.4), i.e. $\nabla_\perp u'(\mathbf{x}^+)\neq\nabla_\perp u'(\mathbf{x}^-)$. Let us introduce the following Hilbert space

$$Z^1_\Sigma(\Omega):=\left\{v(\mathbf{x}):v\in H^1(\Omega_I)\otimes H^1(\Omega_E),\ \text{ s.t. }\int_\Sigma|\nabla_\perp v^+|^2d\sigma+\int_\Sigma[v]^2d\sigma<\infty\right\}. \tag{3.31}$$

We also define $\kappa(\mathbf{x})$ as the mean curvature of Σ (seen as a $n-1$ manifold embedded in $\mathbb{R}^n$) at $\mathbf{x}\in\Sigma$. We now state the main result of this paper, which allows us to characterize the shape derivative of u:

Theorem 3.2. *Assume that $\mathcal{D}(\mathbf{x})$, $a(\mathbf{x})$ and $d(\mathbf{x})$ are functions of class C^1. Then the shape derivative $u' \in Z^1_\Sigma(\Omega)$ of the solution $u \in H^1_\Sigma(\Omega)$ to (2.1) in direction $\mathbf{V}$, is the unique solution of*

$$\begin{aligned}(\mathcal{D}\nabla u', \nabla\phi)_{(\Omega)} + (au', \phi)_{(\Omega)} + (d\nabla_\perp u'^+, \nabla_\perp\phi)_{(\Sigma)} \\ = -(d\mathrm{div}_\Sigma \mathbf{V}_\perp \nabla_\perp u, \nabla_\perp\phi)_{(\Sigma)} - (d\kappa V_n \nabla_\perp u, \nabla_\perp\phi)_{(\Sigma)} \\ - (\mathbf{V}_\perp \cdot \nabla_\perp d\nabla_\perp u, \nabla_\perp\phi)_{(\Sigma)} + (\mathbf{V}\cdot\nabla u^+, \nabla_\perp \cdot d\nabla_\perp\phi)_{(\Sigma)} \\ - (d\mathbf{A}_0'\nabla_\perp u, \nabla_\perp\phi)_{(\Sigma)} + (\mathbf{V}_\perp\cdot\nabla_\perp\phi, \nabla\cdot d\nabla_\perp u)_{(\Sigma)},\end{aligned} \tag{3.32}$$

for all $\phi \in H^1_\Sigma(\Omega)$. Moreover, the jump of u' across Σ is given by

$$[u'] = -[\mathbf{V}\cdot\nabla u]. \tag{3.33}$$

We remark that, thanks to the above jump conditions, (3.32) still holds if the following substitutions are performed:

$$\begin{aligned}(d\nabla_\perp u'^+, \nabla_\perp\phi)_{(\Sigma)} &\to (d\nabla_\perp u'^-, \nabla_\perp\phi)_{(\Sigma)}, \\ (\mathbf{V}\cdot\nabla u^+, \nabla_\perp\cdot d\nabla_\perp\phi)_{(\Sigma)} &\to (\mathbf{V}\cdot\nabla u^-, \nabla_\perp\cdot d\nabla_\perp\phi)_{(\Sigma)}.\end{aligned} \tag{3.34}$$

We also remark that the source term (right-hand side) in (3.32) only involves terms defined on Σ. This is natural, for all other constitutive parameters of (2.1) are kept independent of t, and should be contrasted with the results obtained in (3.29) for the material derivative in Lagrangian coordinates.

Proof (Proof of Theorem 3.2). First, replacing $\dot{u}$ in (3.30) by $u' + \mathbf{V}\cdot\nabla u$ yields the jump condition of u' across the interface, (3.33). Similar replacements in (3.29) lead to

$$\begin{aligned}(\mathcal{D}\nabla u', \nabla\phi)_{(\Omega)} + (au', \phi)_{(\Omega)} + (d\nabla_\perp u'^+, \nabla_\perp\phi)_{(\Sigma)} = -(\mathcal{D}\nabla(\mathbf{V}\cdot\nabla u), \nabla\phi)_{(\Omega)} \\ - ((\mathbf{V}\cdot\nabla\mathcal{D})\nabla u, \nabla\phi)_{(\Omega)} - (\mathcal{D}(J_0'\mathbf{I} + \mathbf{A}_0')\nabla u, \nabla\phi)_{(\Omega)} - (a\mathbf{V}\cdot\nabla u, \phi)_{(\Omega)} \\ - (\nabla\cdot(a\mathbf{V})u, \phi)_{(\Omega)} - ((\mathbf{V}_\perp\cdot\nabla_\perp d)\nabla_\perp u, \nabla_\perp\phi)_{(\Sigma)} - (d\mathrm{div}_\Sigma\mathbf{V}\nabla_\perp u, \nabla_\perp\phi)_{(\Sigma)} \\ - (d\nabla_\perp(\mathbf{V}\cdot\nabla u^+), \nabla_\perp\phi)_{(\Sigma)} - (d\mathbf{A}_0'\nabla_\perp u, \nabla_\perp\phi)_{(\Sigma)}.\end{aligned} \tag{3.35}$$

We then verify by integrations by parts that

$$\begin{aligned}(\mathcal{D}(J_0'\mathbf{I} + \mathbf{A}_0')\nabla u, \nabla\phi)_{(\Omega)} = (\mathcal{D}\nabla\cdot\mathbf{V}\nabla u, \nabla\phi)_{(\Omega)} - (\mathcal{D}\nabla(\mathbf{V}\cdot\nabla u), \nabla\phi)_{(\Omega)} \\ + (\mathcal{D}(\mathbf{V}\cdot\nabla)\nabla u, \nabla\phi)_{(\Omega)} - (\mathcal{D}(\nabla u\cdot\nabla)\mathbf{V}, \nabla\phi)_{(\Omega)}.\end{aligned} \tag{3.36}$$

This implies the following:

$$\begin{aligned}(\mathcal{D}\nabla(\mathbf{V}\cdot\nabla u), \nabla\phi)_{(\Omega)} + (\mathbf{V}\cdot\nabla\mathcal{D}\nabla u, \nabla\phi)_{(\Omega)} + (\mathcal{D}(J_0'\mathbf{I} + \mathbf{A}_0')\nabla u, \nabla\phi)_{(\Omega)} \\ = (\nabla\cdot(\mathcal{D}\nabla u), \mathbf{V}\cdot\nabla\phi)_{(\Omega)} - (\mathbf{V}_\perp\cdot\nabla_\perp\phi, \nabla\cdot d\nabla_\perp u)_{(\Sigma)}.\end{aligned} \tag{3.37}$$

The terms on the boundary $\Gamma = \partial\Omega$ vanish because $\mathbf{V}$ has compact support in Ω. Thanks to the above identity, (3.35) may be recast as

$$\begin{aligned}
&(\mathcal{D}\nabla u', \nabla\phi)_{(\Omega)} + (au', \phi)_{(\Omega)} + (d\nabla_\perp u'^{+}, \nabla_\perp\phi)_{(\Sigma)} \\
&\quad = -(\nabla\cdot(\mathcal{D}\nabla u), \mathbf{V}\cdot\nabla\phi)_{(\Omega)} - (\mathbf{V}\cdot\nabla a u, \phi)_{(\Omega)} - (a\mathbf{V}\cdot\nabla u, \phi)_{(\Omega)} - (aJ_0' u, \phi)_{(\Omega)} \\
&\qquad - ((\mathbf{V}_\perp\cdot\nabla_\perp d)\nabla_\perp u, \nabla_\perp\phi)_{(\Sigma)} - (d\mathrm{div}_\Sigma\mathbf{V}\nabla_\perp u, \nabla_\perp\phi)_{(\Sigma)} \\
&\qquad + (\mathbf{V}\cdot\nabla u^+), \nabla_\perp\cdot d\nabla_\perp\phi)_{(\Sigma)} \\
&\qquad - (d\mathbf{A}_0'\nabla_\perp u, \nabla_\perp\phi)_{(\Sigma)} + (\mathbf{V}_\perp\cdot\nabla_\perp\phi, \nabla\cdot d\nabla_\perp u)_{(\Sigma)}.
\end{aligned} \tag{3.38}$$

Further integrations by parts in (2.1) allow us to show that

$$-(\nabla\cdot(\mathcal{D}\nabla u), \mathbf{V}\cdot\nabla\phi)_{(\Omega)} - (\mathbf{V}\cdot\nabla a u, \phi)_{(\Omega)} - (a\mathbf{V}\cdot\nabla u, \phi)_{(\Omega)} - (aJ_0' u, \phi)_{(\Omega)} = 0. \tag{3.39}$$

These lengthy calculations and combined with the following result[39]

$$\mathrm{div}_\Sigma\mathbf{V} = \mathrm{div}_\Sigma\mathbf{V}_\perp + \kappa V_n \tag{3.40}$$

finally yield (3.32). □

Remark 3.1. In some applications (including the analysis of clear layers in optical tomography[6,8]), it may be necessary to generalize the above calculations to the situation where the tangential diffusion coefficient d depends on the geometry of the interface; for instance via its curvature. In that case, we have to impose that $d(\mathbf{x})$, assumed to be known, is shape differentiable with respect to Σ_t. Theorem 3.2 then still holds provided that we add the term $-(d'\nabla_\perp u, \nabla_\perp\phi)_\Sigma$ to the right-hand side in (3.32). Although this may not be as relevant practically, similar generalizations are possible to the case where $\mathcal{D}(\mathbf{x})$ and $a(\mathbf{x})$ also depend on the geometry of the interface.

The calculation of the material and shape derivatives of the solution u to (2.1) can also be done with model (2.13). We provide the following result without detailing its derivation. Similar results when $\mathcal{D}$ and $\delta\mathcal{D}$ are constant can be found elsewhere.[27,28,39]

Theorem 3.3. *Assume that $\mathcal{D}(\mathbf{x})$ and $a(\mathbf{x})$ are functions of class C^1. Then the material derivative $\dot{u} \in H^1$ of the solution u to Eq.* (2.13) *is the unique solution to*

$$\begin{aligned}
&(\mathcal{D}\nabla\dot{u}, \nabla\phi)_{(\Omega)} + (a\dot{u}, \phi)_{(\Omega)} \\
&\qquad = -(\mathbf{V}\cdot\nabla\mathcal{D}\nabla u, \nabla\phi)_{(\Omega)} - (\mathcal{D}\mathbf{A}_0'\nabla u, \nabla\phi)_{(\Omega)} - (\nabla\cdot(a\mathbf{V})u, \phi)_{(\Omega)}
\end{aligned} \tag{3.41}$$

for all $\phi \in H^1_\Sigma(\Omega)$. The shape derivative of $u' \in H^1$ of $u \in H^1$ then satisfies

$$(\mathcal{D}\nabla u', \nabla\phi)_{(\Omega)} + (au', \phi)_{(\Omega)} = -(\delta\mathcal{D}V_n\nabla_\perp u, \nabla_\perp\phi)_{(\Sigma)} \tag{3.42}$$

for all $\phi \in H^1_\Sigma(\Omega)$.

The proof of this theorem is very similar to that of Theorem 3.2 except that we have to replace identity (3.37) by

$$\begin{aligned}(\mathcal{D}\nabla(\mathbf{V}\cdot\nabla u),\nabla\phi)_{(\Omega)} + ((J_0'\mathbf{I}+\mathbf{A}_0')\mathcal{D}\nabla u,\nabla\phi)_{(\Omega)} + (\mathbf{V}\cdot\nabla\mathcal{D}\nabla u,\nabla\phi)_{(\Omega)}\\ = (\nabla\cdot(\mathcal{D}\nabla u),\mathbf{V}\cdot\nabla\phi)_{(\Omega)} + (\delta\mathcal{D}V_n\nabla_\perp u,\nabla_\perp\phi)_{(\Sigma)}.\end{aligned} \tag{3.43}$$

Remark 3.2. The method based on the map in (3.1) that we have adopted in the paper is not the only choice for shape sensitivity analysis. An *a priori* more general method called the speed (or velocity) method consists of defining the transform $\mathbf{F}_t$ by $\mathbf{F}_t = \mathbf{X}(\mathbf{x},t)$ with $\mathbf{X}(\mathbf{x},t)$ the solution of the following equation:

$$\begin{aligned}&\dot{\mathbf{X}}(t,\mathbf{x}) = \mathbf{V}(t,\mathbf{X}(t,\mathbf{x})),\\ &\mathbf{X}(0,\mathbf{x}) = \mathbf{x}.\end{aligned} \tag{3.44}$$

It has been shown that the velocity method and the transform method used in this paper are actually equivalent in the sense that under sufficient regularity conditions, it is possible to associate a unique velocity field to a given transform $\mathbf{F}_t$ and vice versa.[39]

Remark 3.3. The calculations obtained in the preceding two sections show that the Banach space $B(\Omega)$ may be chosen as the Hilbert $H^1_\Sigma(\Omega)$ in Definition 3.2 of the material derivative for model (2.1) and as $H^1(\Omega)$ for model (2.13); this is because $[\dot{u}] = 0$ across Σ. In both cases, thanks to estimates of the form $C_k(t) \le Ct$ for a constant C in (3.21), we can show that convergence occurs for the strong topology.

The definition of the space $B(\Omega)$ in Definition 3.1 is the same for model (2.13). It is however more complicated for model (2.1). Because u' jumps across Σ, it is not an element of $H^1(\Omega)$, let alone $H^1_\Sigma(\Omega)$. We can however choose $B(\Omega) = L^2(\Omega)$ and observe that convergence in (3.2) is strong in that space. The singular interface model (2.1) introduces singularities that are not present in the inclusion model (2.13).

4. Choosing the Direction of Descent

The analysis presented in the last section enables us to compute the sensitivity of the error functional (4.1) to geometric changes in the interface. Since the vector field $\mathbf{V}(\mathbf{x})$ in (3.1) has compact support, the boundary Γ stays unaffected by perturbations in the interface. We can thus obtain the Eulerian derivative of the error functional as

$$d\mathcal{F}_\alpha(\Sigma) := \lim_{t\to 0}\frac{\mathcal{F}_\alpha(\Sigma_t)-\mathcal{F}_\alpha(\Sigma)}{t} = (u-u_m^\delta,u')_{(\Gamma)} + \alpha(\kappa(\mathbf{x}),V_n)_{(\Sigma)}. \tag{4.1}$$

The second term comes from[27,39]:

$$\left(\frac{d}{dt}\int_{\Sigma_t} d\sigma_t(\mathbf{x})\right)\Big|_\Sigma = \int_\Sigma \kappa(\mathbf{x})V_n d\sigma(\mathbf{x}). \tag{4.2}$$

We recall that $\kappa(\mathbf{x})$ is the mean curvature of the interface Σ at $\mathbf{x}\in\Sigma$.

Since we want the error functional (2.12) to decrease as the interface moves, we need to find a vector field $\mathbf{V}$ such that $d\mathcal{F}_\alpha(\Sigma) \leq 0$. Let us denote by w the solution to the following adjoint equation

$$\begin{aligned} -\nabla \cdot \mathcal{D}(\mathbf{x})\nabla w(\mathbf{x}) + a(\mathbf{x})w(\mathbf{x}) &= 0 && \text{in } \Omega\backslash\Sigma, \\ \mathcal{D}(\mathbf{x})\nu(\mathbf{x}) \cdot \nabla w(\mathbf{x}) &= u - u_m^\delta && \text{on } \Gamma, \\ [w] &= 0 && \text{on } \Sigma, \\ [\mathbf{n} \cdot \mathcal{D}\nabla w] &= -\nabla_\perp \cdot d(\mathbf{x})\nabla_\perp w(\mathbf{x}) && \text{on } \Sigma. \end{aligned} \tag{4.3}$$

Upon multiplying (4.3) by u', performing an integration by parts and taking into account the fact that u' jumps across the interface, we obtain that

$$\begin{aligned} &(\mathcal{D}\nabla w, \nabla u')_{(\Omega)} + (aw, u')_{(\Omega)} + (d\nabla_\perp w, \nabla_\perp u'^+)_{(\Sigma)} \\ &\quad = (u - u_m^\delta, u')_{(\Gamma)} - ([u'], \mathcal{D}\mathbf{n} \cdot \nabla w^-)_{(\Sigma)}. \end{aligned} \tag{4.4}$$

We also observe that the solution of (4.3) belongs to H^1_Σ. Replacing the test function ϕ in (3.32) by w, we obtain

$$\begin{aligned} &(\mathcal{D}\nabla u', \nabla w)_{(\Omega)} + (au', w)_{(\Omega)} + (d\nabla_\perp u'^+, \nabla_\perp w)_{(\Sigma)} \\ &\quad = -(d\mathrm{div}_\Sigma \mathbf{V}_\perp \nabla_\perp u, \nabla_\perp w)_{(\Sigma)} - (d\kappa V_n \nabla_\perp u, \nabla_\perp w)_{(\Sigma)} \\ &\qquad + (\mathbf{V} \cdot \nabla u^+, \nabla_\perp \cdot d\nabla_\perp w)_{(\Sigma)} - (\mathbf{V}_\perp \cdot \nabla_\perp d\nabla_\perp u, \nabla_\perp w)_{(\Sigma)} \\ &\qquad - (d\mathbf{A}_0' \nabla_\perp u, \nabla_\perp w)_{(\Sigma)} + (\mathbf{V}_\perp \cdot \nabla_\perp w, \nabla \cdot d\nabla_\perp u)_{(\Sigma)}. \end{aligned} \tag{4.5}$$

The above equations (4.4) and (4.5) imply that

$$\begin{aligned} (u - u_m^\delta, u')_{(\Gamma)} &= ([u'], \mathcal{D}\mathbf{n} \cdot \nabla w^-)_{(\Sigma)} - (d\mathrm{div}_\Sigma \mathbf{V}_\perp \nabla_\perp u, \nabla_\perp w)_{(\Sigma)} \\ &\quad - (d\kappa V_n \nabla_\perp u, \nabla_\perp w)_{(\Sigma)} - (\mathbf{V}_\perp \cdot \nabla_\perp d\nabla_\perp u, \nabla_\perp w)_{(\Sigma)} \\ &\quad + (\mathbf{V} \cdot \nabla u^+, \nabla_\perp \cdot d\nabla_\perp w)_{(\Sigma)} - (d\mathbf{A}_0' \nabla_\perp u, \nabla_\perp w)_{(\Sigma)} \\ &\quad + (\mathbf{V}_\perp \cdot \nabla_\perp w, \nabla \cdot d\nabla_\perp u)_{(\Sigma)}. \end{aligned} \tag{4.6}$$

Since the tangential component of $\mathbf{V}$ does not affect the evolution of the interface,[36,39] we can assume that the vector field $\mathbf{V}_{|\Sigma}$ is normal to Σ, i.e., $\mathbf{V}_{\perp|\Sigma} = \mathbf{0}$. Then a combination of (4.1) and (4.6) yields

$$\begin{aligned} d\mathcal{F}_\alpha(\Sigma) &= (V_n \nabla_\perp \cdot d\nabla_\perp u, \mathbf{n} \cdot \nabla w^-)_{(\Sigma)} + (V_n \mathbf{n} \cdot \nabla u^+, \nabla_\perp \cdot d\nabla_\perp w)_{(\Sigma)} \\ &\quad - (V_n d\kappa \nabla_\perp u, \nabla_\perp w)_{(\Sigma)} + (\alpha\kappa, V_n)_{(\Sigma)}. \end{aligned} \tag{4.7}$$

Using the interface conditions in (2.1) and (4.3) we can further simplify the above equality as

$$d\mathcal{F}_\alpha(\Sigma) = (V_n, -d\kappa \nabla_\perp u \cdot \nabla_\perp w - \mathbf{n} \cdot \nabla u^+ \mathbf{n} \cdot \mathcal{D}\nabla w^+ + \mathbf{n} \cdot \nabla u^- \mathbf{n} \cdot \mathcal{D}\nabla w^+ + \alpha\kappa)_{(\Sigma)}. \tag{4.8}$$

It remains to choose $\mathbf{V}$ such that $d\mathcal{F}_\alpha(\Sigma) \leq 0$. For the singular surface model (2.1) and the model of inclusion (2.13), we show the following result.

Proposition 4.1. *For the model in* (2.1), *the functional* $\mathcal{F}_\alpha(\Sigma)$ *given in* (2.12) *will not increase if the interface moves according to a vector field characterized by*

$$V_n = d\kappa \nabla_\perp u \cdot \nabla_\perp w + \mathbf{n} \cdot \nabla u^+ \mathbf{n} \cdot \mathcal{D} \nabla w^+ - \mathbf{n} \cdot \nabla u^- \mathbf{n} \cdot \mathcal{D} \nabla w^- - \alpha\kappa, \tag{4.9}$$

where u *and* w *solve* (2.1) *and* (4.3), *respectively. For the model given by* (2.13), *the functional* $\mathcal{F}_\alpha(\Sigma)$ (2.12) *is non-increasing if the interface* Σ *moves in the direction*

$$V_n = -\Big(\delta \mathcal{D} \nabla_\perp u \cdot \nabla_\perp w + \alpha\kappa\Big), \tag{4.10}$$

where u *solves* (2.13) *and* w *solves the adjoint problem*:

$$\begin{aligned} -\nabla \cdot \mathcal{D}(\mathbf{x}) \nabla w(\mathbf{x}) + a(\mathbf{x}) w(\mathbf{x}) &= 0 && \text{in } \Omega, \\ \mathcal{D}(\mathbf{x}) \nu(\mathbf{x}) \cdot \nabla w(\mathbf{x}) &= u - u_m^\delta && \text{on } \Gamma, \\ [w] &= 0 && \text{on } \Sigma, \\ [\mathbf{n} \cdot \mathcal{D} \nabla w] &= 0 && \text{on } \Sigma, \end{aligned} \tag{4.11}$$

with the diffusion coefficient $\mathcal{D}(\mathbf{x})$ *given by* (2.14).

Note that (4.10) is the well-known result for the inverse obstacle problem obtained by shape sensitivity analysis.[9,27,28,35] Allowing the diffusion coefficient $\mathcal{D}$ to be spatially dependent in model (2.13) does not modify the choice of a velocity field. In the inverse problem for singular surfaces, both the geometry of the surface (via its mean curvature κ) and the tangential diffusion process it carries, enter non-trivially in the choice of the vector field given in (4.9).

5. Level Set Implementation

Once the direction of descent has been chosen, we need an efficient way to move the interface along that direction. We use here the level set method[29,32] to do so. The level set method represents interfaces as the zero level sets of level set functions and then moves of the interfaces implicitly by solving a Hamilton-Jacobi equation for the level set functions. The application of the level set method to shape optimization problem has been pioneered by Santosa[35] and further studied by many authors.[2,9,12,27] We refer to the recent monographs[29,30,37] and their references therein for a detailed account of the method and its many applications.

5.1. *Representing and moving interfaces*

Let Σ_t be an evolution interface in $\Omega \subset \mathbb{R}^n$ viewed as the zero level set of a function $\psi(\mathbf{x}, t)$:

$$\Sigma_t := \{\mathbf{x} : \mathbf{x} \in \Omega, \text{ such that } \psi(\mathbf{x}, t) = 0\}. \tag{5.1}$$

To track the position of the interface Σ_t, we evaluate the derivative of $\psi(\mathbf{x}(t), t) = 0$ with respect to t to obtain

$$\frac{\partial \psi}{\partial t} + \dot{\mathbf{x}}(t) \cdot \nabla \psi = \frac{\partial \psi}{\partial t} + \mathbf{V} \cdot \nabla \psi = 0, \tag{5.2}$$

where $\mathbf{V}$ is the velocity field at the interface. Since the tangential velocity does not affect the evolution of the interface,[36] we can choose $\mathbf{V}_\perp = \mathbf{0}$. Using the fact that

the normal vector of the interface can be written as $\mathbf{n}(\mathbf{x}) = \nabla\psi/|\nabla\psi|$, we arrive at

$$\frac{\partial\psi}{\partial t} + V_n|\nabla\psi| = 0. \tag{5.3}$$

This is a nonlinear transport equation of the Hamilton-Jacobi form. Let us now suppose that we know an approximate position for the interface and the normal velocity V_n at a given "time step". Then by solving this Hamilton-Jacobi equation, we can compute the position of the interface at the following "time step".

5.2. *Implementation of the level set method*

The level set method is implemented numerically as follows. We focus on the two-dimensional setting to simplify the calculations.

Algorithm:

- $L1$. We choose an initial level set function $\psi^0(\mathbf{x})$, such that the interface can be represented as $\Sigma_0 = \{\mathbf{x} : \mathbf{x} \in \Omega, \psi^0(\mathbf{x}) = 0\}$, and set $k = 0$;
- $L2$. We solve the state equation (2.1) (resp. (2.13)) with the interface $\Sigma_k = \{\mathbf{x} : \mathbf{x} \in \Omega, \psi^k(\mathbf{x}) = 0\}$;
- $L3$. We compare the solution with given measurements. If a stopping criteria is satisfied, we stop the calculation. Otherwise:
- $L4$. We solve the adjoint equation (4.3) (resp. 4.11)) to compute the normal velocity V_n on Σ_k by (4.9) (resp. (4.10)). We extend the velocity field to a computational tube around Σ by using (5.7) below;
- $L5$. We move the interface Σ_k to a new interface Σ_{k+1} by updating the Hamilton–Jacobi equation (5.3) by one time step Δt;
- $L6$. We re-initialize the level set function according to Eq. (5.10) if necessary;
- $L7$. We set $k := k + 1$ and go back to step $L2$.

Here are additional details about the implementation. The Hamilton–Jacobi equation (5.3) has been discretized by using the following first-order scheme[29]

$$\frac{\psi_{i,j}^{n+1} - \psi_{i,j}^n}{\Delta t} + \max(V_{i,j}^n, 0)H_+ + \min(V_{i,j}^n, 0)H_- = 0, \tag{5.4}$$

where the superscript n and subscript i, j denote time and space grid point, respectively. The numerical Hamiltonians H_+ and H_- are given by

$$\begin{aligned} H_+ &= \sqrt{\max(a,0)^2 + \min(b,0)^2 + \max(c,0)^2 + \min(d,0)^2}, \\ H_- &= \sqrt{\min(a,0)^2 + \max(b,0)^2 + \min(c,0)^2 + \max(d,0)^2}, \end{aligned} \tag{5.5}$$

with

$$\begin{aligned} a \equiv D_x^- \psi_{i,j}^n &:= \frac{\psi_{i,j}^n - \psi_{i-1,j}^n}{\Delta x}, \quad b \equiv D_x^+ \psi_{i,j}^n := \frac{\psi_{i+1,j}^n - \psi_{i,j}^n}{\Delta x}, \\ c \equiv D_y^- \psi_{i,j}^n &:= \frac{\psi_{i,j}^n - \psi_{i,j-1}^n}{\Delta y}, \quad d \equiv D_y^+ \psi_{i,j}^n := \frac{\psi_{i,j+1}^n - \psi_{i,j}^n}{\Delta y}. \end{aligned} \tag{5.6}$$

The time step Δt is chosen so small as to satisfy the CFL stability condition. The surface Σ_k is updated to Σ_{k+1} after each iteration of the Hamilton–Jacobi equation and the vector field is updated according to (4.9).

The vector field V_n in (4.9) is only defined at the interface Σ. We need to extend it in the neighborhood of Σ to solve the Hamilton–Jacobi equations. This is done by using the following two-way extrapolation, equation[13]

$$V_t + S(\psi)\frac{\nabla\psi}{|\nabla\psi|}\cdot\nabla V = 0, \tag{5.7}$$

where the sign function is defined as

$$S(\psi) = \begin{cases} -1 & \text{if } \psi < 0, \\ 0 & \text{if } \psi = 0, \\ +1 & \text{if } \psi > 0. \end{cases} \tag{5.8}$$

A detailed discussion can be found elsewhere.[29] Equation (5.7) is solved as follows[33]:

$$\begin{aligned} &\frac{V_{ij}^{n+1} - V_{ij}^n}{\Delta t} + \max(S_{ij}n_{ij}^x, 0)D_x^- V_{ij}^n + \min(S_{ij}n_{ij}^x, 0)D_x^+ V_{ij}^n \\ &\quad + \max(S_{ij}n_{ij}^y, 0)D_y^- V_{ij}^n + \min(S_{ij}n_{ij}^y, 0)D_y^+ V_{ij}^n = 0, \end{aligned} \tag{5.9}$$

over a time interval of roughly 5–10 times Δt, where $D_x^{\pm}V_{ij}^n$ and $D_y^{\pm}V_{ij}^n$ are finite differences defined as in (5.6). The sign function $S(\psi)$ is approximated by $\frac{\psi}{\sqrt{\psi^2+\delta^2}}$ with δ a small regularization parameter. The directions $\hat{n} = (n^x, n^y) = \left(\frac{\psi_x}{\sqrt{\psi_x^2+\psi_y^2}}, \frac{\psi_y}{\sqrt{\psi_x^2+\psi_y^2}}\right)$ are computed by a central difference scheme.

Finally, we comment on the re-initialization process (step $L6$ in the above algorithm). The level set function may become very flat or very steep near the interface Σ. To avoid this, we replace the level set function $\psi(\mathbf{x}, t)$ by $d(\mathbf{x}, t)$ which is the value of the signed distance from $\mathbf{x}$ to Σ. The quantity $d(\mathbf{x}, t)$ satisfies the Eikonal equation $|\nabla d| = 1$, and is the steady state solution of the following re-initialization equation

$$\begin{aligned} \frac{\partial\psi}{\partial t} + S(\psi_0)(|\nabla\psi| - 1) = 0 \quad &\text{in } \Omega\times(0,+\infty) \\ \psi(\mathbf{x}, t) = \psi_0 \quad &\text{in } \Omega\times\{0\}. \end{aligned} \tag{5.10}$$

A stationary solution of (5.10) is obtained by choosing t large enough.[29,40] Here we approximate the function $S(\psi_0)$ by $\frac{\psi_0}{\sqrt{\psi_0^2+|\nabla\psi_0|^2\Delta x^2}}$ as suggested before.[33] The numerical scheme for Eq. (5.10) is given by[33]:

$$\frac{\psi_{ij}^{n+1} - \psi_{ij}^n}{\Delta t} + \max(S_{ij}, 0)(H_+ - 1) + \min(S_{ij}, 0)(H_- - 1), \tag{5.11}$$

where $H_{\pm}$ are defined as in (5.5). In the examples shown in the next section, we reinitialize the level set function every ten time steps.

6. Numerical Simulations

In this section, we numerically invert the singular surface problem (2.1) and the inclusion's support problem (2.13) by using shape derivative analysis and the level set method. We consider the two-dimensional setting and the domain $\Omega = (-1, 1) \times (-1, 1)$. This domain is discretized by a uniform 401×401 grid on which all the Hamilton–Jacobi equations are solved by using the finite difference schemes described above and the elliptic equations (2.1) and (4.3) during the iterative process are solved by the finite element method on rectangular elements[10] and a nonlinear conjugate gradient solver. All the numerical minimizations of the error functional (4.1) presented in this paper are performed with the optimal choice of the regularization parameter α obtained by the Morozov discrepancy principle.[19]

The synthetic data are calculated by solving (2.1) and (4.3) by a finite element method on an unstructured triangulation with approximately the same number of nodes as the uniform grid mentioned above. The only common nodes of the two set of meshes are the boundary nodes where the measurements are taken. We have checked that the systematic error between the solutions on the uniform mesh and the fined unstructured mesh is far below 0.05%. The synthetic measurements have been obtained by a different numerical procedure than what is being used in the reconstruction algorithm to limit the occurence of "inverse crimes", where the minimization of the un-penalized functional (4.1) with $\alpha = 0$ may return the correct answer for the wrong reasons; see Ref. 14 for an account of this problem.

In all simulations, we have chosen the diffusion coefficients to be $(\mathcal{D}, d) = (1.0, 0.3)$ in model (2.1) and $(\mathcal{D}_0, \delta\mathcal{D}) = (1.0, 3.0)$ in model (2.13). The absorption coefficient $a = 0$ in both models. The values taken by these parameters have a significant impact on the reconstruction. This will be discussed briefly at the end of this section.

6.1. *Reconstructions of ellipses*

We start with the simple example where Ω_I is an ellipse. Note that in real applications such as optical imaging of human brain, we may be allowed to approximate clear layers by such simple convex interfaces. The ellipse we want to reconstruct is given in polar coordinate by

$$\Sigma = \left\{ (r, \theta) : \left(\frac{r \cos\theta}{a} \right)^2 + \left(\frac{r \sin\theta}{b} \right)^2 = 1 \right\}, \tag{6.1}$$

with a and b the semi-major and semi-minor axis length, respectively. We test our algorithm with different values for (a, b).

To characterize the error in the reconstruction, we introduce the following Fourier decomposition of $r(\theta)$:

$$r(\theta) = \sum_{k=-N}^{N} c_k e^{-ik\theta}, \tag{6.2}$$

where we have chosen $N = 20$ in the following calculations. The complexity of the curve will be measured by the magnitude of the Fourier coefficients c_k and their decay rate as k increases. Let $\tilde{c}_k$ be the Fourier coefficients of a reconstructed interface. We then define the ε_0 and ε_{-1} errors between the original and the reconstructed interfaces as

$$\varepsilon_0 = \left(\sum_{k=-N}^{N} |c_k - \tilde{c}_k|^2 \right)^{1/2} \quad \text{and} \quad \varepsilon_{-1} = \left(\sum_{k=-N}^{N} (1+k^2)^{-1} |c_k - \tilde{c}_k|^2 \right)^{1/2}, \quad (6.3)$$

respectively.

The reconstruction results from different additive noise levels in the case $(a, b) = (0.8, 0.4)$ are given in Fig. 2. The left column of Fig. 2 shows the reconstructions

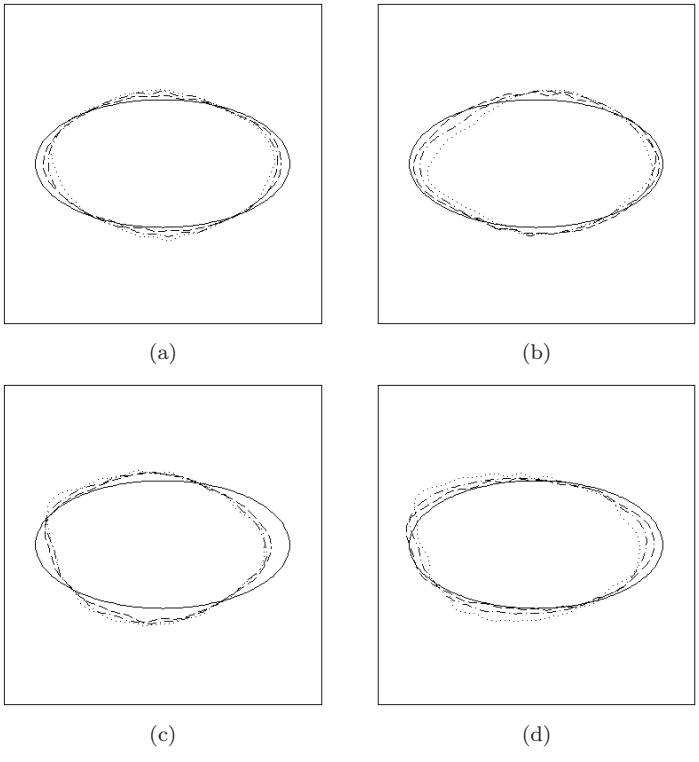

Fig. 2. Reconstruction of the elliptic interface (6.1) with synthetic data at different noise levels for full (top row) and local (bottom row; see text for description) Neumann-to-Dirichlet measurements. We have $(a, b) = (0.8, 0.4)$. The reconstructions in (a) and (c) are done with the model in (2.1), while those in (b) and (d) are done with the model in (2.13). The lines in the pictures denote real interfaces (solid), reconstructions from data with 0.5% additive noise (dashed), reconstructions from data with 1% additive noise (dash-dotted) and reconstructions from data with 2% additive noise (dotted), respectively. The initial guess is given by the circle $\Sigma_0 = \{(r, \theta) : (r\cos\theta)^2 + (r\sin\theta)^2 = 0.8^2\}$ in all the simulations.

for the model (2.1) from full and local Neumann-to-Dirichlet measurements. In the latter case, measurements are only taken on the left side ($x = -1$) of the boundary. We have used the MATLAB contour function to plot the zero level set (characterizing the interface Σ) of the level set function. All the simulations have been implemented in Fortran 77. The same reconstructions have been performed for the model (2.13) and the results are show in the right column of Fig. 2.

We list in Tables 1 and 2 the errors in the reconstructions of ellipses of different aspect ratios using model (2.1) with full and partial Neumann-to-Dirichlet measurements, respectively. Note that the closer the aspect ratio $\frac{b}{a}$ is to 1.0, the less Fourier modes are needed to accurately represent $r(\theta)$. From these tables we see that as the aspect ratio increases, the reconstructions get more and more sensitive to the presence of noise in the data. In the reconstructions from full data, the center of the curves is relatively stably reconstructed even in the presence of significant noise. In the case of local measurements on part of the boundary, the reconstructed center of the ellipse is biased towards the part of the boundary where the boundary measurements are taken.

Table 1. Errors in the reconstructions of ellipses (6.1) with different values of (a, b) using model (2.1) with full measurements. The center of original interfaces $(x_0, y_0) = (0, 0)$.

Cases		0.5%	1.0%	2.0%
$(a, b) = (0.8, 0.4)$	$(x_0,\ y_0)$	(0.001, 0.000)	(−0.001, −0.002)	(−0.001, −0.001)
	ε_0	0.037	0.057	0.078
	ε_{-1}	0.008	0.011	0.015
$(a, b) = (0.8, 0.6)$	$(x_0,\ y_0)$	(0.002, 0.000)	(−0.002, 0.002)	(−0.003, 0.001)
	ε_0	0.011	0.020	0.031
	ε_{-1}	0.003	0.004	0.006
$(a, b) = (0.8, 0.8)$	$(x_0,\ y_0)$	(−0.000, −0.002)	(0.017, 0.006)	(0.000, 0.009)
	ε_0	0.005	0.015	0.017
	ε_{-1}	0.001	0.004	0.004

Table 2. Same as Table 1 except that the reconstructions are obtained from partial measurements.

Cases		0.5%	1.0%	2.0%
$(a, b) = (0.8, 0.4)$	$(x_0,\ y_0)$	(−0.039, −0.013)	(−0.047, −0.017)	(−0.057, −0.016)
	ε_0	0.076	0.098	0.104
	ε_{-1}	0.018	0.026	0.040
$(a, b) = (0.8, 0.6)$	$(x_0,\ y_0)$	(−0.015, 0.008)	(−0.013, 0.008)	(0.013, 0.009)
	ε_0	0.035	0.052	0.076
	ε_{-1}	0.014	0.018	0.020
$(a, b) = (0.8, 0.8)$	$(x_0,\ y_0)$	(−0.030, 0.010)	(−0.031, 0.006)	(−0.045, 0.004)
	ε_0	0.019	0.029	0.048
	ε_{-1}	0.007	0.011	0.019

6.2. *Reconstruction of more complicated surfaces*

The reconstructions in the above section are all done with ellipses, which are convex interfaces. The Fourier coefficients of those interfaces decay relatively fast as k increases. The reconstruction of such curves is thus not very difficult because the superposition of very few low-order Fourier modes can approximate the original interface quite accurately and those low-order Fourier modes can be stably reconstructed from data with even moderately high noise level. We now reconstruct more complicated interfaces the representation of which require higher-order Fourier modes. Since high order modes are more sensitive to the presence of noise in the data, we expect such interfaces to be harder to reconstruct. For simplicity, we reconstruct here star-shaped interfaces given by

$$\Sigma = \{(r,\theta) : r^2 + 0.3r\sin(N\theta) = 0.6^2\}. \tag{6.4}$$

Several choices for N are considered in the reconstructions below.

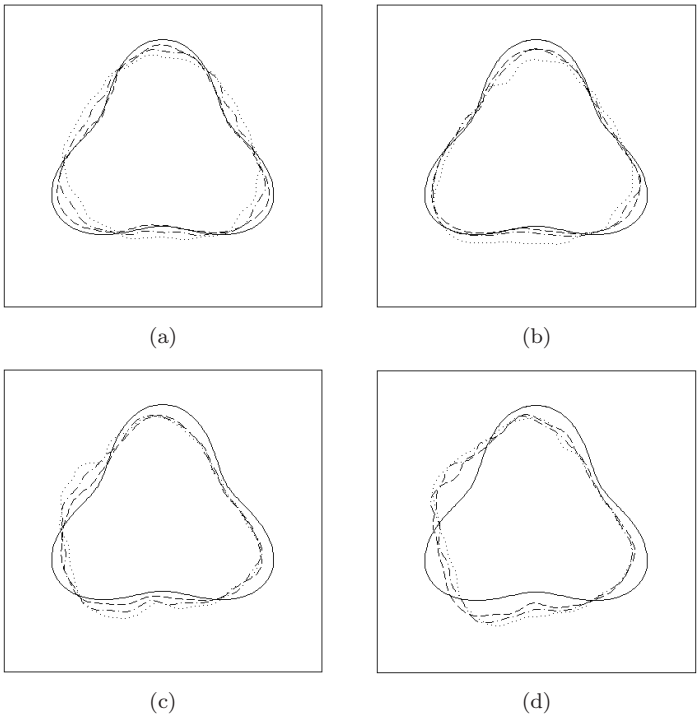

Fig. 3. Reconstruction of the star-shaped interface (6.4) from synthetic data with different noise levels in the case of full (top row) and local (bottom row) Neumann-to-Dirichlet measurements. The interface parameter is $N = 3$. The reconstructions in (a) and (c) are for model (2.1), while those in (b) and (d) are for model (2.13). The lines in the pictures denote real interfaces (solid), reconstructions with 0.1% noise (dashed), reconstructions with 0.3% noise (dash-dotted) and reconstructions with 0.5% noise (dotted), respectively. The initial guess is the circle $\Sigma_0 = \{(r,\theta) : (r\cos\theta)^2 + (r\sin\theta)^2 = 0.8^2\}$.

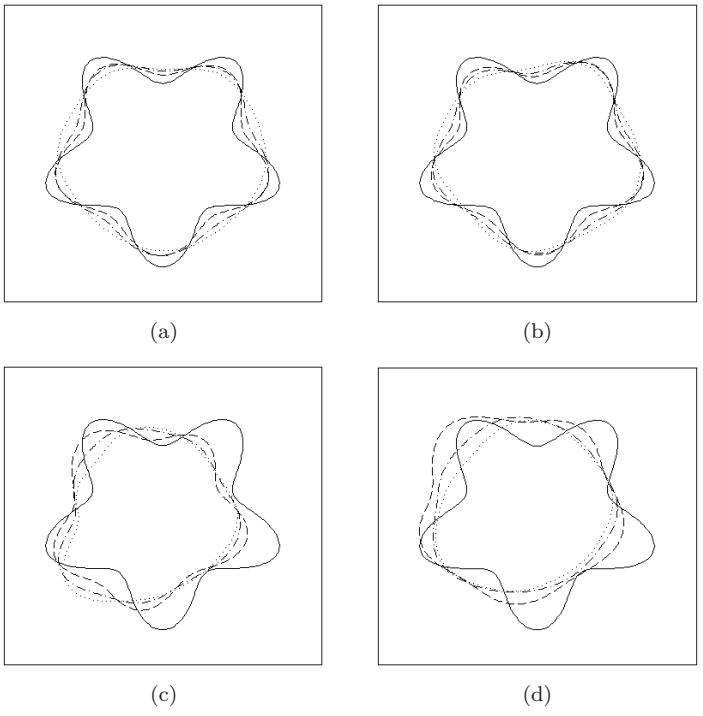

Fig. 4. Same as in Fig. 3 except that $N = 5$.

We show in Figs. 3 and 4 reconstructions with $N = 3$ and $N = 5$, respectively, using synthetic data at different noise levels for full (top row) and local (bottom row) Neumann-to-Dirichlet measurements. Again, we use only the left side ($x = -1$) of the boundary for the local measurements. The errors in these reconstructions are shown by the parameters presented in Table 3 and Fig. 5.

The latter reconstructions are more sensitive to noise in the data than those in the preceding section although the centers of the interfaces are always relatively well reconstructed when full measurements are available.

We observe in our numerical experiments that the ratios of the parameters, $d/\mathcal{D}$ and $\mathcal{D}_0/\delta\mathcal{D}$, have important effects on the reconstruction results. The bigger the ratio, the more stable the reconstruction. This is simply because the effect of the interface on the boundary measurements increases. Note, however, that when the ratio $d/\delta\mathcal{D}$ is large, the conjugate gradient method used to calculate the solution of (2.1) converges very slowly. This is because the conditioning number of the finite element matrix in model (2.1) significantly increases when the ratio increases. For this reason, we have chosen the values $(\mathcal{D},\ d) = (1.0,\ 0.3)$ to save computational time. Larger values of d would require to find an efficient preconditioner if solutions are to be obtained in a reasonable computational time. Indeed our simulations, based on the Morozov discrepancy principle[19] to find the optimal regularization parameter α, are very demanding computationally.

Table 3. Reconstructed centers for the cases presented in Figs. 3 ($N = 3$) and 4 ($N = 5$).

Cases		0.5%	1.0%	2.0%
Model (2.1), $N = 3$	Full	(0.000, 0.0110)	(−0.005, 0.017)	(−0.003, 0.022)
	Local	(−0.029, −0.015)	(−0.046, −0.023)	(−0.053, −0.031)
Model (2.13), $N = 3$	Full	(−0.001, 0.003)	(−0.003, −0.017)	(−0.013, −0.046)
	Local	(−0.054, −0.028)	(−0.056, −0.028)	(−0.063, −0.031)
Model (2.1), $N = 5$	Full	(0.000, −0.007)	(0.001, −0.018)	(0.002, −0.018)
	Local	(−0.061, 0.013)	(−0.067, 0.019)	(−0.084, 0.018)
Model (2.13), $N = 5$	Full	(0.010, −0.006)	(0.012, −0.012)	(0.017, −0.015)
	Local	(−0.065, +0.022)	(−0.099, 0.022)	(−0.081, 0.021)

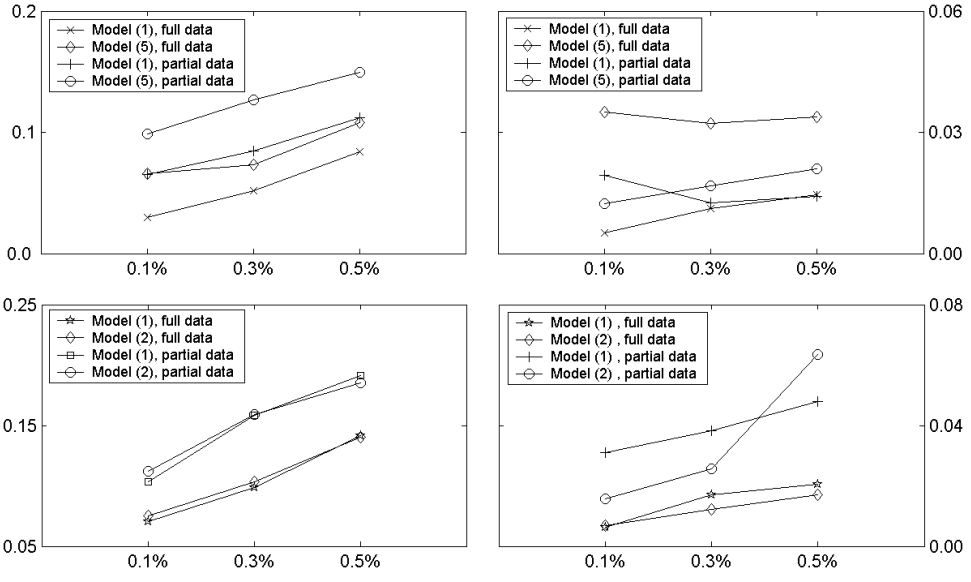

Fig. 5. Errors in the reconstructions of (6.4) for different noise levels and different parameters N. Upper left: ε_0 and $N = 3$; Upper right: ε_{-1} and $N = 3$; Bottom left: ε_0 and $N = 5$; Bottom right: ε_{-1} and $N = 5$.

7. Conclusions and Discussions

We have considered the reconstruction of singular surfaces in diffusion models arising in optical and electrical impedance tomography. We have performed a shape sensitivity analysis to describe the effects of variations in the surface on the boundary measurements. We have obtained that such effects primarily depended on the mean curvature of surface and the value of the tangential diffusion process supported on the surface. This is in contrast to the classical case of discontinuous diffusion coefficients across an interface.

We have introduced a level set method to evolve the surface so as to minimize an error functional. We have shown numerically that the reconstruction of the low-order Fourier modes of the interface can be achieved quite accurately from moderately noisy data. Higher frequency modes require less noisy data. The reconstructions can be done from either full or local Neumann-to-Dirichlet measurements although full measurements obviously provide more accurate reconstructions.

The major drawback of the current method is that it requires the diffusion coefficient $d(\mathbf{x})$ to be known. Generalizations, for instance along the lines of the works of Chan and Tai,[12] to reconstructions of both the interface and the tangential diffusion coefficient need to be addressed. Note that in such a context, the coefficient $d(\mathbf{x})$ will depend on the geometric properties of the interface Σ (see Remark 3.1 and many previous works[6,8,25]).

Acknowledgments

We would like to thank the anonymous referee for his/her constructive comments on the first version of this paper. We also acknowledge useful discussions with Martin Burger (Johannes Kepler Universität Linz, Austria) and Stanley Osher (UCLA) on the implementation of the level set method. Martin Burger also pointed out an important reference[21] when reading the first version of this paper. This work was funded in part by NSF grant DMS-0239097. G.B. acknowledges support from an Alfred P. Sloan fellowship.

References

1. R. A. Adams, *Sobolev Spaces* (Academic Press, 1975).
2. G. Allaire, F. Jouve and A. M. Toader, Structural optimization using sensitivity analysis and a level set method, *J. Comput. Phys.* **194** (2004) 363–393.
3. L. Ambrosio and G. Buttazzo, An optimal design problem with perimeter penalization, *Calc. Var.* **1** (1993) 55–69.
4. S. R. Arridge, Optical tomography in medical imaging, *Inverse Problems* **15** (1999) R41–R93.
5. S. R. Arridge, H. Dehghani, M. Schweiger and E. Okada, The finite element model for the propagation of light in scattering media: A direct method for domains with nonscattering regions, *Med. Phys.* **27** (2000) 252–264.
6. G. Bal, Transport through diffusive and non-diffusive regions, embedded objects, and clear layers, *SIAM J. Appl. Math.* **62** (2002) 1677–1697.
7. G. Bal, Reconstructions in impedance and optical tomography with singular interfaces, *Inverse Problems* **21** (2005) 113–131.
8. G. Bal and K. Ren, Generalized diffusion model in optical tomography with clear layers, *J. Opt. Soc. Am. A* **20** (2003) 2355–2364.
9. H. Ben Ameur, M. Burger and B. Hackl, Level set methods for geometric inverse problem in linear elasticity, *Inverse Problems* **20** (2004) 673–696.
10. S. C. Brenner and L. R. Scott, *The Mathematical Theory of Finite Element Methods* (Springer-Verlag, 1994).
11. M. Burger and S. J. Osher, A survey on level set methods for inverse problems and optimal design, *Euro. J. Appl. Math.* **16** (2005) 263–301.

12. T. F. Chan and X.-C. Tai, Level set and total variation regularization for elliptic inverse problems with discontinuous coefficients, *J. Comput. Phys.* **193** (2003) 40–66.
13. S. Chen, B. Merriman, S. Osher and P. Smereka, A simple level set method for solving stefan problems, *J. Comput. Phys.* **135** (1997) 8–29.
14. D. Colton and R. Kress, *Inverse Acoustic and Electromagnetic Scattering Theory* (Springer-Verlag, 1998).
15. G. Dal Maso and R. Toader, A model for the quasi-static growth of brittle fractures: Existence and approximation results, *Arch. Rational Mech. Anal.* **162** (2002) 101–135.
16. R. Dautray and J.-L. Lions, *Mathematical Analysis and Numerical Methods for Science and Technology* (Springer-Verlag, 1993), Vol. 2.
17. F. Desaint and J.-P. Zolésio, Shape derivatives for the Laplace-Beltrami equation, in *Partial Differential Equation Methods in Control and Shape Analysis*, eds. G. D. Prato and J.-P. Zolésio (Marcel Dekker, 1997).
18. O. Dorn, Shape reconstruction in scattering media with void using a transport model and level sets, *Canad. Appl. Math. Quart.* **10** (2001) 239–275.
19. H. W. Engl, M. Hanke and A. Neubauer, *Regularization of Inverse Problems* (Kluwer, 1996).
20. W. Fang and K. Ito, Identification of contact regions in semiconductor transistors by level-set methods, *J. Comput. Appl. Math.* **159** (2003) 399–410.
21. J. Ferchichi and J.-P. Zolésio, Shape sensitivity for the Laplace–Beltrami operator with singularities, *J. Diff. Eqns.* **196** (2004) 340–384.
22. M. Firbank, S. R. Arridge, M. Schweiger and D. T. Delpy, An investigation of light transport through scattering bodies with non-scattering regions, *Phys. Med. Biol.* **41** (1996) 767–783.
23. D. Gilbarg and N. S. Trudinger, *Elliptic Partial Differential Equations of Second Order* (Springer-Verlag, 2000).
24. J. Haslinger and P. Neittanmaaki, *Finite Element Approximation for Optimal Shape, Material and Topology Design*, 2nd edn. (John Wiley and Sons, 1996).
25. P. H. Hung and E. Sánchez-Palencia, Phénomènes de transmission à travers des couches minces de conductivité élevée, *J. Math. Anal. Appl.* **47** (1974) 284–309.
26. V. Isakov, *Inverse Problems for Partial Differential Equations* (Springer-Verlag, 1998).
27. K. Ito, K. Kunisch and Z. Li, Level set function approach to an inverse interface problem, *Inverse Problems* **17** (2001) 1225–1242.
28. A. Litman, D. Lesselier and F. Santosa, Reconstruction of a two-dimensional binary obstacle by controlled evolution of a level-set, *Inverse Problems* **14** (1998) 685–704.
29. S. Osher and R. Fedkiw, *Level Set Methods and Dynamic Implicit Surfaces* (Springer-Verlag, 2002).
30. S. Osher and N. Paragios (eds.), *Geometric Level Set Methods in Imaging, Vision, and Graphics* (Springer-Verlag, 2003).
31. S. J. Osher and F. Santosa, Level set methods for optimization problems involving geometry and constraints I. Frequencies of a two-density inhomogeneous drum, *J. Comput. Phys.* **171** (2001) 272–288.
32. S. J. Osher and J. A. Sethian, Front propagation with curvature-dependent speed: Algorithms based on Hamilton–Jacobi formulations, *J. Comput. Phys.* **79** (1988) 12–49.
33. D. Peng, B. Merriman, S. Osher, H. Zhao and M. Kang, A PDE-based fast local level set method, *J. Comput. Phys.* **155** (1999) 410–438.

34. J. Ripoll, M. Nieto-Vesperinas, S. R. Arridge and H. Dehghani, Boundary conditions for light propagation in diffusive media with nonscattering regions, *J. Opt. Soc. Am. A* **17** (2000) 1671–1682.
35. F. Santosa, A level-set approach for inverse problems involving obstacles, *ESAIM: Control, Optim. Calculus Variations* **1** (1996) 17–33.
36. G. Sapiro, *Geometric Partial Differential Equations and Image Analysis* (Cambridge Univ. Press, 2001).
37. J. A. Sethian, *Level Set Methods and Fast Marching Methods* (Cambridge Univ. Press, 1999).
38. J. Simon, Differentiation with respect to the domain in boundary value problems, *Numer. Funct. Anal. Optim.* **2** (1980) 649–687.
39. J. Sokolovski and J. P. Zolésio, *Introduction to Shape Optimization* (Springer, 1992).
40. M. Sussman, P. Smereka and S. Osher, A levelset approach for computing solutions to incompressible two-phase flow, *J. Comput. Phys.* **114** (1994) 146–159.